Subharmonic behavior of phospholipid-coated ultrasound contrast agent microbubbles

Jeroen Sijl
Physics of Fluids Group and MIRA Institute of Biomedical Engineering and Technical Medicine, University of Twente, P. O. Box 217, 7500 AE Enschede, The Netherlands

Benjamin Dollet
Institut de Physique de Rennes, UMR 6251, CNRS/Université de Rennes 1, Campus Beaulieu, Bâtiment 11A, 35042 Rennes Cedex, France

Marlies Overvelde
Physics of Fluids Group and MIRA Institute of Biomedical Engineering and Technical Medicine, University of Twente, P.O. Box 217, 7500 AE Enschede, The Netherlands

Valeria Garbin
Department of Chemical and Biomolecular Engineering, University of Pennsylvania, Room 311A, Towne Building, 330 South 33rd St., Philadelphia, Pennsylvania 19104

Timo Rozendal
Physics of Fluids Group, University of Twente, P. O. Box 217, 7500 AE Enschede, The Netherlands

Nico de Jong
Biomedical Engineering, Erasmus MC, P.O. Box 2040, 3000 CA Rotterdam, The Netherlands

Detlef Lohse and Michel Versluis[a)]
Physics of Fluids Group and MIRA Institute of Biomedical Engineering and Technical Medicine, University of Twente, P.O. Box 217, 7500 AE Enschede, The Netherlands

(Received 18 February 2010; revised 26 August 2010; accepted 31 August 2010)

Coated microbubbles, unlike tissue are able to scatter sound subharmonically. Therefore, the subharmonic behavior of coated microbubbles can be used to enhance the contrast in ultrasound contrast imaging. Theoretically, a threshold amplitude of the driving pressure can be calculated above which subharmonic oscillations of microbubbles are initiated. Interestingly, earlier experimental studies on coated microbubbles demonstrated that the threshold for these bubbles is much lower than predicted by the traditional linear viscoelastic shell models. This paper presents an experimental study on the subharmonic behavior of differently sized individual phospholipid coated microbubbles. The radial subharmonic response of the microbubbles was recorded with the Brandaris ultra high-speed camera as a function of both the amplitude and the frequency of the driving pulse. Threshold pressures for subharmonic generation as low as 5 kPa were found near a driving frequency equal to twice the resonance frequency of the bubble. An explanation for this low threshold pressure is provided by the shell buckling model proposed by Marmottant *et al.* [J. Acoust. Soc. Am. **118**, 3499–3505 (2005)]. It is shown that the change in the elasticity of the bubble shell as a function of bubble radius as proposed in this model, enhances the subharmonic behavior of the microbubbles. © *2010 Acoustical Society of America.* [DOI: 10.1121/1.3493443]

PACS number(s): 43.80.Qf, 43.80.Vj, 43.35.Ei, 43.35.Yb [CCC] Pages: 3239–3252

I. INTRODUCTION

Microbubbles scatter ultrasound effectively and non-linearly, which makes them ideal contrast agents for medical ultrasound imaging. The bubbles are coated with a protein, lipid or polymer layer and they are filled with air or an inert gas. Ultrasound contrast agents are clinically used on a daily basis to visualize blood flow at the microvascular level to image organ perfusion in e.g. the liver, kidney and the myocardium.[1–4] Contrast enhancement can be expressed as the ratio between the response of microbubbles in the blood pool and that of the surrounding tissue, termed the contrast-to-tissue ratio (CTR), see e.g., Ref. 5. Improvement of the CTR for current contrast imaging modalities such as power modulation[6] and pulse inversion imaging[7] is accomplished by exploiting the non-linear response of the microbubbles, predominantly at the second harmonic frequency of the driving frequency.[8,9]

The typical enhancement of the CTR in non-linear harmonic imaging is 40 dB. For deep tissue imaging, however, the contrast enhancement is limited by the non-linear propagation of the ultrasound. Linear scattering of the second harmonic component of the propagating wave, by tissue, inter-

[a)]Author to whom correspondence should be addressed. Electronic mail: m.versluis@utwente.nl

feres with the bubbles second harmonic response. On the other hand, no subharmonic components of the driving frequency are generated during propagation. For this reason the subharmonic response of the bubbles at half the driving frequency has received increased interest for ultrasound contrast imaging.[10] Moreover the subharmonic response is attenuated less than both the fundamental and higher harmonic bubble responses. Currently, the subharmonic response is mostly used in high frequency imaging applications.[11,12]

Subharmonic bubble responses were first described following experimental observations by Esche[13] already in 1952. Additional experimental work has been conducted to investigate the nature of this non-linear behavior[14,15] followed by several theoretical descriptions of subharmonic behavior of bubbles in a sound field.[16–20] Prosperetti[18] showed through a weakly non-linear analysis of the Rayleigh-Plesset equation[21–24] that the subharmonic behavior of bubbles can only exist if the driving pressure amplitude exceeds a threshold pressure. It was found that the threshold pressure for subharmonic behavior is minimum when the bubble is driven at twice its resonance frequency. It was also shown that the threshold pressure increases with increased damping, which is a result of reradiation, thermal losses and the liquid viscosity.[16,18,25]

The viscoelastic shell of ultrasound contrast agent microbubbles is known to increase the damping considerably.[26–28] Therefore, it has always been speculated that the threshold pressure to excite subharmonic behavior for coated microbubbles should increase. Shankar *et al.*[29] studied the subharmonic behavior of coated bubbles following the analysis of Prosperetti[18] and confirmed, by using a purely *linear* viscoelastic shell model as by de Jong *et al.*,[26] Church,[30] or Hoff *et al.*,[31] that indeed the threshold for subharmonic generation is increased as a result of the increased damping. There exists, however, experimental evidence in the literature showing that for both the albumin-coated contrast agents Optison™ and Albunex® and the phospholipid-coated contrast agent SonoVue®, the threshold pressure to excite subharmonic behavior is lower than that of uncoated bubbles.[8,10,29,32–35] Other work reports no significant change in the threshold pressure, not for albumin-coated bubbles[36] nor for the phospholipid-coated Definity™ contrast agent microbubbles.[37]

Here, we show that a lower threshold for the initiation of subharmonic behavior of phospholipid-coated microbubbles can be explained with the model proposed by Marmottant *et al.*[38] Similarly to Shankar *et al.*[29] we employ a weakly non-linear analysis along the earlier work on free bubbles by Prosperetti,[18] and instead of using a purely *linear* viscoelastic model, we assume the shell elasticity of the phospholipid shell to vary with the bubble radius R. It is shown that the rapid change in the elasticity of the bubble shell as proposed in the model of Marmottant *et al.*, is responsible for the enhancement of the non-linear subharmonic behavior of phospholipid-coated ultrasound contrast agent microbubbles. Furthermore we have used ultra high-speed imaging with the Brandaris camera[39] to characterize the subharmonic behavior of individual microbubbles from the experimental agent BR-14, which contains microbubbles with a phospholipid shell and a perfluorocarbon gas core (Bracco Research S.A., Geneva, Switzerland). We have investigated the full subharmonic resonance and threshold behavior of individual coated microbubbles for small acoustic pressures and driving pulse frequencies near two times the resonance frequency of the microbubbles.

Details of the model and the weakly non-linear analysis are presented in Sec. II. The experimental setup is discussed in Sec. III. In Sec. IV the experimental results are presented and compared to the numerical simulations using the model of Marmottant *et al.* Finally we end with a discussion in Sec. V and our conclusions in Sec. VI.

II. THEORY

A. Analytical solution

A general description of the dynamics of phospholipid coated microbubbles is given by Marmottant *et al.*,[38]

$$\rho\left(R\ddot{R}+\frac{3}{2}\dot{R}^2\right)=\left(P_0+\frac{2\sigma(R_0)}{R_0}\right)\left(\frac{R_0}{R}\right)^{3\gamma}\left(1-\frac{3\gamma\dot{R}}{c}\right)-\frac{2\sigma(R)}{R}-4\mu\frac{\dot{R}}{R}-4\kappa_s\frac{\dot{R}}{R^2}-P_0-P_A(t). \quad (1)$$

Here, the radius of the bubble is described by $R(t)$ and its velocity and acceleration are given by $\dot{R}$ and $\ddot{R}$, respectively. The initial bubble radius is given by R_0 and the ambient pressure by P_0. The liquid viscosity is $\mu=10^{-3}$ Pa s, its density $\rho=10^3$ kg/m^3 and the speed of sound in the liquid is $c=1500$ m/s. The applied acoustic pressure pulse is described by $P_A(t)$. We approximate the microbubble oscillations as adiabatic.[28,38] Therefore we assume the polytropic exponent γ to be the ratio of the specific heats of the gas inside the bubble. For the experimental agent BR-14 the gas core consists of perfluorocarbon gas with $\gamma=C_p/C_v=1.07$.[28,38] Thermal damping is accounted for by a slight increase of the liquid viscosity $\mu=2\times10^{-3}$ Pa s.[40,41]

The effect of the phospholipid coating is taken into account through a shell viscosity κ_s and an effective surface tension which is assumed to depend on the concentration of phospholipid molecules on the surface of the bubble. Consequently, the surface tension depends on the radius of the bubble $\sigma(R)$. In earlier models[26,31] the effective surface tension was assumed to increase linearly with the bubble radius, $\sigma(R)=2\chi(R/R_0-1)$, where χ represents the shell elasticity. Based on the static properties of phospholipid monolayers, Marmottant *et al.*[38] introduced a relation for $\sigma(R)$ where also the shell elasticity is varied with bubble radius $\chi(R)$.

To investigate the effect of $\sigma(R)$ on the subharmonic response, Eq. (1) can be solved numerically for different functions $\sigma(R)$. However, to come to a more fundamental understanding of the effect of $\sigma(R)$ on the subharmonic behavior of ultrasound contrast agents it is insightful to solve Eq. (1) analytically. Hereto we perform a weakly non-linear analysis of Eq. (1) where we follow the approach of Prosperetti.[18,19,25,29] The principal steps of the weakly non-linear analysis will be repeated here.

As a most general approximation, we assume that, for small oscillations around R_0, $\sigma(R)$ can be described as a second order Taylor expansion:

$$\sigma(R) = \sigma(R_0) + 2\chi_{\text{eff}}\left(\frac{R}{R_0} - 1\right) + \frac{1}{2}\zeta_{\text{eff}}\left(\frac{R}{R_0} - 1\right)^2, \tag{2}$$

where we have defined for any function $\sigma(R)$,

$$\chi_{\text{eff}} = \frac{1}{2}R_0 \left.\frac{\partial\sigma(R)}{\partial R}\right|_{R_0}, \tag{3}$$

$$\zeta_{\text{eff}} = R_0^2 \left.\frac{\partial^2\sigma(R)}{\partial R^2}\right|_{R_0}. \tag{4}$$

χ_{eff} and ζ_{eff} are the effective shell elasticity and the derivative of the effective shell elasticity around the equilibrium point R_0. In the model of Marmottant *et al.* $\chi(R)$ and $\zeta(R)$ depend on the bubble radius R. The effective shell elasticity χ_{eff} and ζ_{eff} defined in Eqs. (3) and (4), respectively, are constants. The shell elasticity as determined by van der Meer *et al.*[28] for BR-14 microbubbles was assumed to be independent of the bubble radius R and is therefore equal to χ_{eff}.

We can show that the results of the weakly non-linear analysis presented in the following are independent of the choice of the initial surface tension $\sigma(R_0)$. To simplify the calculations presented here we therefore assume $\sigma(R_0)$ to be zero. We insert Eq. (2) into Eq. (1) and assume the radius R of the bubble is correctly described by

$$R = R_0(1 + x), \tag{5}$$

where x is small. Following Prosperetti[18] we define a dimensionless timescale, frequency and driving pressure amplitude:

$$\tau = \sqrt{\frac{P_0}{\rho}}\frac{t}{R_0}, \quad \omega = R_0\Omega\sqrt{\frac{\rho}{P_0}}, \quad \xi = \frac{P_a}{P_0}, \tag{6}$$

where Ω is the dimensional driving frequency and P_a is the driving pressure amplitude. Because we assume the surface tension at rest $\sigma(R_0)$ to be zero, the corresponding pressure inside the bubble is equal to P_0.

Inserting all these relations into Eq. (1), performing a series expansion in x, and ignoring third and higher order terms we obtain

$$\frac{\mathrm{d}^2x}{\mathrm{d}\tau^2} + \omega_0^2 x = -\frac{3}{2}\left(\frac{\mathrm{d}x}{\mathrm{d}\tau}\right)^2 + \alpha_1 x^2 - \xi x\cos(\omega\tau) - 2b\frac{\mathrm{d}x}{\mathrm{d}\tau} + \xi\cos(\omega\tau), \tag{7}$$

where we have assumed the driving pressure to be described by $P_A/P_0 = \xi\cos(\omega\tau)$. Eq. (7) is identical to Eq. (4) from Prosperetti[18] except for the third order terms which we neglect since we are only interested in the solution of this equation for $\omega \approx 2\omega_0$, for which the second-order terms are sufficient.[18] Furthermore we have defined

$$\omega_0^2 = 3\gamma + \frac{4\chi_{\text{eff}}}{P_0R_0}, \tag{8}$$

$$b = \frac{2\mu}{R_0\sqrt{\rho P_0}} + \frac{2\kappa_s}{R_0^2\sqrt{\rho P_0}} + \frac{3\gamma}{2c}\sqrt{\frac{P_0}{\rho}}, \tag{9}$$

$$\alpha_1 = \frac{9}{2}\gamma(\gamma+1) - \frac{\zeta_{\text{eff}} - 8\chi_{\text{eff}}}{P_0R_0}, \tag{10}$$

where b describes the non-dimensional damping of the system. Note that the resonance frequency in dimensional form follows directly from Eq. (8) inserted into Eq. (6). Around $\omega \approx 2\omega_0$ the solution of Eq. (7) reads

$$x = \frac{\xi}{\sqrt{(\omega^2 - \omega_o^2)^2 + 4b^2\omega^2}}\cos(\omega\tau + \delta) + C\cos\left(\frac{1}{2}\omega\tau + \varphi\right), \tag{11}$$

where δ is the phase angle of the linear solution which satisfies

$$\tan\delta = \frac{2b\omega}{\omega^2 - \omega_0^2}. \tag{12}$$

The amplitude of the first subharmonic solution either vanishes ($C=0$), or becomes

$$C = \sqrt{\frac{\omega_o^2 - \frac{1}{4}\omega^2 + g_1\xi^2 + \sqrt{\beta^2\xi^2 - \omega^2b^2}}{g_0}}, \tag{13}$$

where

$$\beta = \left|\frac{1}{2} - \frac{\alpha_1 - \frac{3}{4}\omega^2}{\omega_0^2 - \omega^2}\right|, \tag{14}$$

$$g_0 = \alpha_1\left(\frac{\alpha_1 - \frac{3}{8}\omega^2}{\omega_0^2} + \frac{1}{2}\frac{\alpha_1 + \frac{3}{8}\omega^2}{\omega_0^2 - \omega^2}\right) + \frac{3}{8}\omega^2\left(\frac{1}{4} - \frac{\alpha_1 + \frac{3}{8}\omega^2}{\omega_0^2 - \omega^2}\right), \tag{15}$$

and

$$g_1 = \frac{\alpha_1}{\omega_0^2(\omega_0^2 - \omega^2)}\left(1 - \frac{\alpha_1 - \frac{3}{2}\omega^2}{\omega_0^2 - \omega^2}\right) - \frac{3}{4}\frac{\omega^2}{(\omega_0^2 - \omega^2)^2} - \frac{1}{\omega_0^2 - \omega^2} + \left(\omega_0^2 - \frac{9}{4}\omega^2\right)^{-1}\left(\frac{\alpha_1 + \frac{3}{4}\omega^2}{\omega_0^2 - \omega^2} - \frac{1}{2}\right)\left(\frac{1}{2} - \frac{\alpha_1 - \frac{9}{4}\omega^2}{\omega_0^2 - \omega^2}\right). \tag{16}$$

Theoretically the solution of Eq. (13) can only exist if the term $\beta^2\xi^2 - \omega^2b^2$ is positive. This corresponds to the well-known theoretical threshold for the existence of subharmonics,

$$\xi_{\text{th}}(\omega) = \frac{\omega b}{\beta}. \tag{17}$$

The threshold determines the regime where the subharmonic solution is stable. However, as discussed by Prosperetti and others[16,25], depending on the initial conditions the subharmonic solution may still not exist. Another threshold is provided by the regime where the linear solution of Eq. (11) becomes unstable. In this regime the only stable solution is the subharmonic solution. The instability threshold, ξ_{in} is given by[16,25]

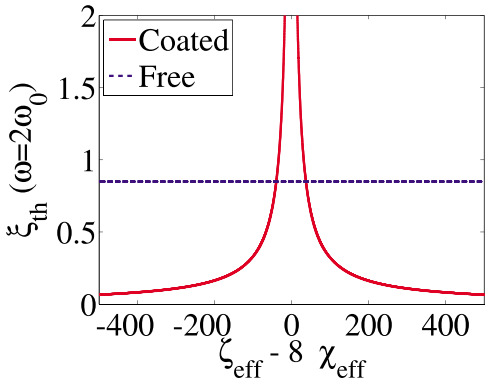

FIG. 1. (Color online) The mathematical threshold ξ_{th} at $\omega/\omega_0=2$ given by Eq. (17) plotted as a function of the term $\zeta_{eff}-8\chi_{eff}$ for $R_0=3.8$ μm with fixed $\chi_{eff}=0.55$ N/m. We observe that if $|\zeta_{eff}-8\chi_{eff}|$ is large enough, the threshold for a coated bubble can decrease below the threshold of a free gas bubble despite its additional shell damping. The damping for the free gas bubble is determined by the reradiation damping and the liquid viscosity, for this bubble $b=0.1$. For the coated bubble model the shell damping introduces and extra damping described by the shell viscosity which is taken 3×10^{-8} kg/s resulting in a total damping of $b_{coated}=0.5$.

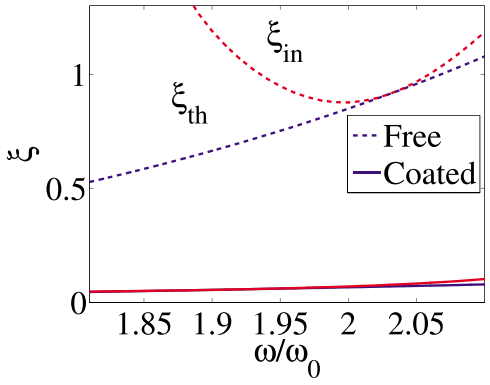

FIG. 2. (Color online) The mathematical threshold ξ_{th} and the instability threshold ξ_{in} as a function of ω/ω_0 for $R_0=3.8$ μm. The damping for the coated and the free bubble are the same as in Fig. 1, i.e., the damping coefficient for the coated bubble is five times as large as for the uncoated bubble. Even so, the threshold for a coated bubble is only 6 kPa, much lower than for an uncoated bubble which has a threshold of 90 kPa. This decrease of the threshold for the coated bubble results from the rapid change of in the effective surface tension as a function of R described by $\chi_{eff}=0.55$ N/m and $\zeta_{eff}=504.4$ N/m ($\zeta_{eff}-8\chi_{eff}=500$ N/m).

$$\xi_{in}(\omega)=\sqrt{\frac{1}{2g_1^2}\left\{\beta^2-2g_1\left(\omega_0^2-\frac{1}{4}\omega^2\right)-\sqrt{\beta^4-4g_1\left[\left(\omega_0^2-\frac{1}{4}\omega^2\right)\beta^2+g_1\omega^2b^2\right]}\right\}^{1/2}}, \tag{18}$$

which for $\omega=2\omega_0$ reduces to $\xi_{in}=\xi_{th}$.

From Eq. (17) it is clear that the threshold for subharmonics increases with increased damping. However, from Eq. (10) and Eq. (14) it follows that β and consequently ξ_{th} vary with $\zeta_{eff}-8\chi_{eff}$. $\zeta_{eff}-8\chi_{eff}$ is determined by the initial condition of the phospholipid shell. In Fig. 1 we have plotted ξ_{th} at $\omega=2\omega_0$ as a function of $\zeta_{eff}-8\chi_{eff}$ for the linearized free gas bubble model from Prosperetti[18] and for the coated bubble model with $\sigma(R)$ described by Eq. (2) for $R_0=3.8$ μm. The damping for the coated bubble is determined by Eq. (9) where we assume the shell viscosity is equal to $\kappa_s=3\times10^{-8}$ kg/s as determined by van der Meer *et al.* for the same type of bubbles.[28] This brings the total damping for the coated bubble to $b_{coated}=0.5$. For the uncoated bubble the damping is determined by the bubble size and γ only, bringing the total damping of the uncoated bubble to $b_{free}=0.1$. We observe that depending on the initial condition of the shell $\zeta_{eff}-8\chi_{eff}$, the threshold for a coated bubble can vary. If $|\zeta_{eff}-8\chi_{eff}|$ is sufficiently large, the threshold for the coated bubble can be lower than the threshold for an uncoated bubble. This provides a possible explanation that even for a fivefold increase of the damping as a result of the shell, the threshold for the existence of subharmonics for coated bubbles can be lower than for uncoated bubbles depending on the initial conditions of the bubble shell.

The ultrasound contrast agent models with a purely elastic shell regime[26,27,30] cannot predict a decrease in the threshold pressure as a function of the initial conditions since in these models ζ_{eff} is either zero or of the same order as χ_{eff}, hence $|\zeta_{eff}-8\chi_{eff}|$ remains about 1 N/m, which is too low to explain subharmonic enhancement for contrast agents. In the shell buckling model proposed by Marmottant *et al.*[38] we can identify that close to the transition point from the elastic to the buckled regime, $\chi(R)$ changes rapidly from $\chi_{max}\approx2.5$ N/m to $\chi=0$ N/m, corresponding to a large $\zeta(R)$. In fact, in the current model of Marmottant *et al.* $\zeta(R)$ is undefined at the transition points. At the transition points $\zeta(R_0)\sim\zeta_{eff}$ can be much higher than $\chi(R_0)\sim\chi_{eff}$, hence $|\zeta_{eff}-8\chi_{eff}|$ can be large enough to enable subharmonic enhancement for contrast agents. In Fig. 2 we have fixed $\chi_{eff}=0.55$ N/m (corresponding to the average shell elasticity χ_{eff} found by van der Meer *et al.*[28] for the same type of bubbles) and $\zeta_{eff}=504.4$ N/m. In Fig. 2 we have plotted both ξ_{th} and ξ_{in} as a function of ω/ω_0 for both the free gas bubble and the coated bubble model with $\sigma(R)$ described by Eq. (2). As a result of the initial conditions we observe that both thresholds (ξ_{th} and ξ_{in}) for a coated microbubble are as low as 6 kPa, much lower than those for a free gas bubble where the threshold is near 90 kPa.

B. Full numerical solution

The analytical solutions presented in the previous section provide a fundamental understanding of the source of subharmonic behavior of coated microbubbles. However, for these calculations we have assumed an infinitely long driving pressure pulse and a sufficiently small amplitude of oscillation neglecting higher order terms in Eq. (7). In practice, the driving pressure pulse has a finite length and the amplitudes of oscillation of the microbubbles exceed the small amplitude limit. In the following we will therefore solve Eq. (1) numerically. Solving the equation numerically requires a model for the relation between the bubble radius and the effective surface tension $\sigma(R)$.

We will assume $\sigma(R)$ to be described as proposed in the model of Marmottant *et al.*[38] In agreement with what is known for the static behavior of phospholipid monolayers, Marmottant *et al.* assume it is the surface concentration of

phospholipids on the surface of the bubble that determines the surface tension experienced by the bubble. For low surface concentrations of phospholipids, the surface tension of the water-air interface of the bubble is unaltered and thus equal to $\sigma_{water}=0.072$ N/m. This regime corresponding to an expanded bubble (area) is referred to as the ruptured regime. If the surface concentration of phospholipids on the surface of the bubble increases for example by compressing the bubble, the surface tension of the bubble decreases and the bubble enters the elastic regime. In the model of Marmottant *et al.* it is assumed that in the elastic regime the surface tension of the bubble varies linearly with the radius of the bubble according to $\sigma(R)=2\chi_{max}(R/R_0-1)$ as in the model of de Jong *et al.*[26] The shell elasticity in the elastic regime is referred to as the maximum shell elasticity χ_{max}. We know from Overvelde *et al.*[42] that the maximum shell elasticity in the elastic regime for these type of microbubbles is $\chi_{max}=2.5$ N/m. Below a certain radius the surface concentration of phospholipids cannot increase more and at this point the bubble enters the buckled regime with a corresponding minimum surface tension of $\sigma(R)=0$. In the model of Marmottant *et al.* the shell elasticity varies with bubble radius from zero in the buckled and ruptured regime to χ_{max} in the elastic regime. The variation of the shell elasticity with bubble radius is defined by $\zeta(R)$, i.e., the derivative of the shell elasticity with respect to R. In the model of Marmottant *et al.* $\zeta(R)$ is undefined near the two transition points from the buckled regime to the elastic regime and from the elastic regime to the ruptured regime. The piecewise affine function introduced by Marmottant *et al.* is a practical idealization of the shell response which is smoother in physical reality.

The smoothening represented by the $\zeta(R)$ parameter can be considered a second-order or non-linear elastic correction. In order to have $\zeta(R)$ defined for all R we assume $\zeta(R)$ in the two transition regimes to be defined by two quadratic functions. A quadratic function is the first order correction on a linearly varying surface tension and requires the introduction of only one new parameter. This modification to the original model of Marmottant *et al.* is described in more detail in the Appendix. The Appendix starts with a more detailed description of the model of Marmottant *et al.* after which the two quadratic functions and their corresponding boundary conditions are introduced. The shell parameters of the model that are undetermined up to now are the initial surface tension $\sigma(R_0)$, the shell viscosity κ_s and finally the value of ζ in the two transition regimes of the effective surface tension. From the theoretical threshold for the existence of subharmonics [Eq. (17)] we expect that these three shell parameters strongly influence the subharmonic behavior. The shell viscosity increases the damping b of the system and is therefore expected to decrease the subharmonic response. On the other hand, the initial surface tension $\sigma(R_0)$ and the quadratic transition determined by ζ strongly affect ζ_{eff} and thus β in Eq. (17).

The effect of $\sigma(R_0)$ on the subharmonic behavior of phospholipid coated microbubbles is shown in Fig. 3. In Fig. 3 two different responses of a 3.8 μm radius bubble driven at an acoustic pressure of 40 kPa with a frequency of 2.4 MHz are shown. We observe that the bubble with a small

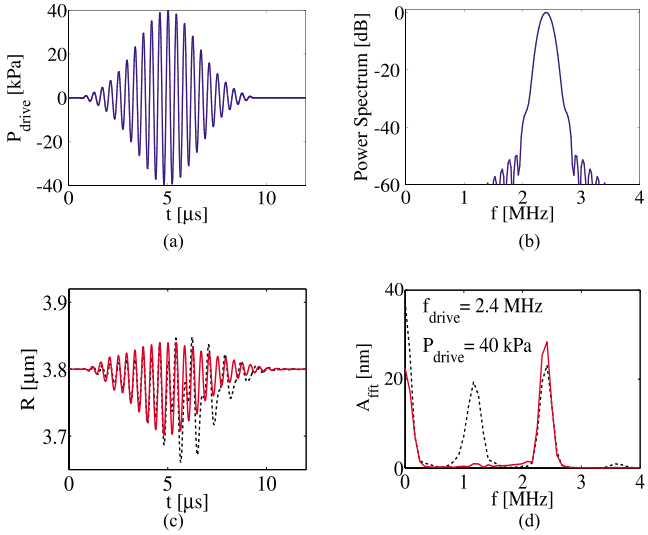

FIG. 3. (Color online) Top figures: An example of the driving pressure waveform (a), and (b) its corresponding power spectrum. Bottom figures: The radius time curve (c) and the corresponding Fourier transform amplitude A_{FFT} (d) for two bubbles with a different initial surface tension $\sigma(R_0)$ driven with a driving pressure pulse of 40 kPa with a frequency of 2.4 MHz. The dotted line represents the numerical simulation for a bubble with $\sigma(R_0)=0.001$ N/m and the solid line corresponds to a bubble with $\sigma(R_0)=0.01$ N/m. The initial bubble radius and the other shell parameters are the same for both bubbles, $\zeta=2000$ N/m, $\kappa_s=3\times10^{-8}$ kg/s and $\chi_{max}=2.5$ N/m.

initial surface tension, $\sigma(R_0)$ close to the buckled regime shows a large subharmonic response. In contrast, for a bubble with an initial surface tension in the elastic regime no subharmonic response is observed. Note also that the fundamental response for both bubbles is similar and is almost unaffected by $\sigma(R_0)$.

To investigate the effect of the shell parameters on the subharmonic behavior, a parametric study was conducted. The results are shown in Fig. 4. In the parametric study the driving pulse pressure amplitude and frequency were kept constant at 40 kPa and 2.4 MHz, respectively. The driving frequency corresponds to two times the resonance frequency of the bubble. The corresponding pulse shape of the driving pressure pulse is shown in Fig. 3(a) and is the same as was used in the experiments which will be discussed in the next section. The initial bubble radius was 3.8 μm and it was found that the results presented in Fig. 4 are similar for all bubbles with an initial bubble radius between 1 μm and 5 μm. Finally, while one of the shell parameters was varied the other four parameters were fixed as in Fig. 3, i.e., $\sigma(R_0)=0.001$ N/m, $\zeta=2000$ N/m, $\kappa_s=3\times10^{-8}$ kg/s and $\chi_{max}=2.5$ N/m.

The fundamental response in all three cases in Fig. 4 is observed to vary little as compared to the subharmonic response which strongly depends on shell parameters. The subharmonic threshold is observed to strongly depend on the damping κ_s. In Fig. 4(b) we observe that for $\kappa_s=6\times10^{-8}$ kg/s the threshold for the initiation of subharmonics is 40 kPa corresponding to the driving pressure amplitude. For smaller κ_s the subharmonic response is observed to increase. In agreement with what was found in the weakly non-linear analysis we find that the subharmonic response

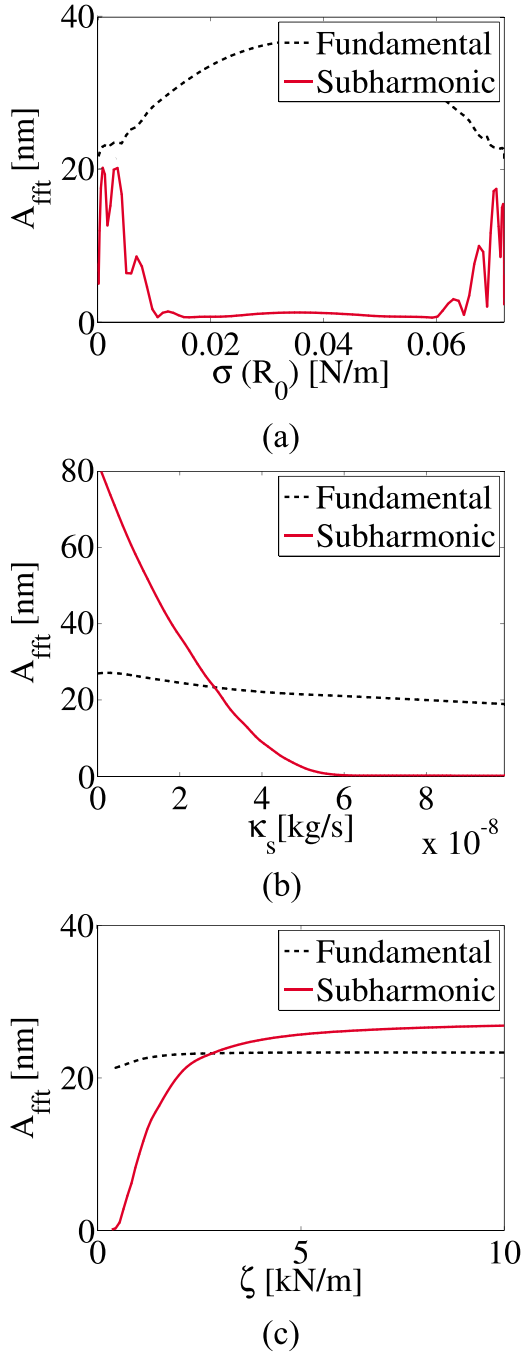

FIG. 4. (Color online) The absolute value of the Fourier transforms of a parametric study on the simulated radius-time curve presented in Fig. 3. The fundamental response to the driving pressure of 2.4 MHz is clearly visible in all three figures while the subharmonic response is observed to strongly vary for each shell parameter varied independently. (a) For $\sigma(R_0)$ varied between 0 and σ_{water} the subharmonic response is only visible for the initial condition of the bubble satisfying $\sigma(R_0)\approx 0$ or $\sigma(R_0)\approx\sigma_{water}$. (b) As expected the subharmonic response is observed to decrease for κ_s increasing from 0 to 10^{-7} kg/s and (c) for ζ increasing from 342 to 10 000 N/m the subharmonic is observed to increase but for $\zeta > 5000$ N/m the amplitude of the subharmonic response saturates.

depends strongly on the change of the initial shell elasticity. Indeed, the subharmonic behavior is only observed for microbubbles that have an initial surface tension close to $\sigma(R_0)\approx 0$ or $\sigma(R_0)\approx\sigma_{water}$, close to the transitions from the elastic regime to the two other regimes corresponding to a large second derivative of the effective surface tension. The local minima observed in the subharmonic response in Fig. 4(a) are a result of transient effects resulting from the finite length of the driving pressure pulse. These local minima disappear for an increased length of the driving pressure pulse. As with the linearized model we can conclude that the change in the effective surface tension is of fundamental importance to be able to predict subharmonic behavior for phospholipid coated microbubbles at low driving pressure amplitudes. Furthermore, a difference in the initial surface tension of bubbles caused by the initial phospholipid surface concentration explains why in some experiments subharmonics are observed at low driving pressures while in other experiments no subharmonics are observed for microbubbles similar to the ones used in this study.[10,29,32–35,37,38]

Finally, the subharmonic response is also observed to increase with increasing ζ; see Fig. 4(c). For an increased ζ also $\zeta_{eff}=2R_0(\partial(\chi(R_0))/\partial R)$ increases, provided $\sigma(R_0)\approx 0$. The transition from the elastic regime to the other two regimes becomes sharper. Following Fig. 1 such an increase would result in a decrease of the threshold for the generation of subharmonics. The maximum subharmonic response is observed to saturate for a value of $\zeta > 5000$ N/m. Based on the experimental relation between surface tension and phospholipid surface concentration found in the literature (see e.g., Wen and Franses[43] and Cheng and Chang[44]) the magnitude of ζ is expected to be at least three orders of magnitude larger than the elasticity χ in order to explain the abrupt elasticity change found for collapsing phospholipid monolayers. With ζ of order 1000 N/m and χ of order 1 N/m, this is indeed the case in our study.

III. EXPERIMENTAL

The previous sections have shown that the subharmonic behavior of phospholipid coated bubbles is predominantly determined by the driving pulse frequency, pressure amplitude, and the initial phospholipid surface concentration of the microbubble. Experimentally, the initial phospholipid surface concentration of the phospholipid shell of the microbubble is difficult to control as opposed to the frequency and the amplitude of the driving pulse. We therefore have recorded the radial dynamics of 39 different isolated microbubbles with the Brandaris ultra high-speed camera[39] as a function of both the driving pressure pulse frequency and amplitude.

A. Setup

The experimental setup is schematically shown in Fig. 5. The setup consists of a cylindrical Plexiglass container that was mounted under an upright microscope (BXFM, Olympus Optical, Japan). Within the container the microbubbles were confined inside an OptiCell cell culture chamber (Thermo Fisher Scientific, Waltham, MA, USA). The acoustic transmit circuit consists of a focused 3-MHz center frequency transducer (PA168, Precision Acoustics Ltd., Dorset, U.K.) that was mounted under an angle of 45° under the OptiCell. A 0.2 mm needle hydrophone (Precision Acoustics Ltd., Dorset, U.K.) that moves in and out of the combined optical and acoustical focus was used to calibrate and align

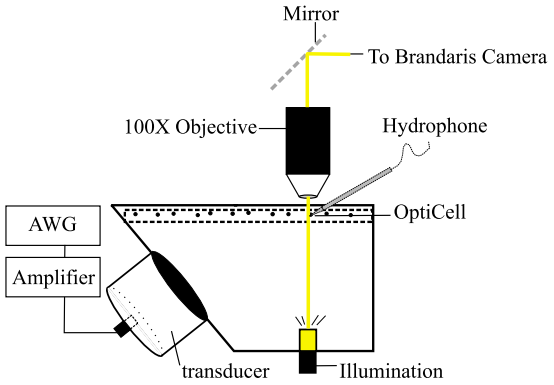

FIG. 5. (Color online) A schematic overview of the experimental setup that was used to optically record the radial dynamics of coated microbubbles located inside an optically and acoustically transparent OptiCell chamber. The driving pressure waveform produced by an arbitrary waveform generator (AWG) was amplified and transmitted by a focused transducer. The radial dynamics were recorded through a 100× objective coupled through an inverted microscope into the Brandaris ultra high-speed camera.

the transducer. The transmit transducer was excited with a sequence of pulses generated by an arbitrary waveform generator (Tabor Electronics Ltd., Model 8026, Haifa, Israel) and amplified by a power amplifier (ENI, Model 350L with 50 Ω input impedance, Rochester, NY). To calibrate and align the transmit transducer, a broadband chirp function was used to excite the transducer. The output response of the transducer was measured with the calibrated needle hydrophone in the focus of the transducer. From the response the transmit transfer function of the transducer was determined as is described in Ref. 45.

The optical focus of a 100× microscope objective was positioned in the acoustical focus of the transducer. It was illuminated from below with a high intensity xenon flashlight (MVS 7010 XE, Perkin Elmer, Waltham, MA). A continuous-wave light source (ACE I, Schott, NY) in combination with a CCD camera (LCL-902K, Qwonn) was used to monitor the bubble in between experiments. The image plane of the microscope objective was coupled into the Brandaris 128 ultra high speed imaging facility. The high-speed camera consists of 128 separate highly sensitive CCD (Charge Coupled Device) sensors that are illuminated consecutively by a rotating mirror. The mirror turbine is driven by a mass-flow controlled flow of Helium, at a revolving rate of up to 20,000 revolutions per second, corresponding to a frame rate of 25 million frames per second. Six consecutive movies of 128 frames each can be stored in a memory buffer with a time interval of 80 ms. We employed the microbubble spectroscopy method detailed in Ref. 28 to characterize the bubbles. The microbubbles were excited with a smoothly windowed driving pressure waveform with a frequency ranging from 1 to 4 MHz, all with peak rarefactional amplitudes ranging from 5 to 150 kPa and a fixed length of 8.9 μs. An example of a driving pressure waveform is shown in Fig. 3(a). In preparation of the experiment 12 driving pressure pulses were uploaded to the arbitrary waveform generator. The frequencies of each of the waveforms were varied and equally spaced near two times the resonance frequency of the microbubble. In this way the radial subharmonic resonance behavior of the bubble was quantified. The optical recordings consisted of two times six movies at a frame rate near 13 Mfps. The movies were stored on a PC, and all data were post-processed using Matlab (The Mathworks, Natick, MA). The image sequence of the oscillating bubble was analyzed with Matlab through a semi-automatic minimum cost algorithm[28] to give the radius of the bubble as a function of time $R(t)$.

All the results discussed in this paper were conducted with microbubbles located against the top wall of the OptiCell. The experimental setup is compatible with an optical tweezers setup that was coupled through the microscope into the microscope objective. With this combined setup we could also position the microbubbles 100 μm away from the top wall. The details of this setup are described in full detail in previous work.[46,47] To investigate the effect of the wall on the subharmonic behavior of coated microbubbles we have conducted several scans around the subharmonic resonance of different microbubbles both when the bubble was located against the top wall of the OptiCell and when brought 100 μm away from the wall. Based on these experiments we conclude that the presence of a wall does not alter the subharmonic behavior of ultrasound contrast agents to be experimentally observable in the current setup. In the following we therefore only consider the results based on the setup without the optical tweezers.

IV. RESULTS

In total, 39 individual microbubbles were included in this study. Subharmonic responses were observed for approximately 50% of the microbubbles. The other 50% of the microbubbles could not be forced into subharmonic oscillations for the driving pressure amplitudes and/or pulse lengths employed in this study which were always smaller than 150 kPa. This finding confirms previous results by Bhagavatheeshwaran *et al.*[36] and by Kimmel *et al.*[37] In those cases where subharmonic oscillations were observed these were initiated already at driving pressure amplitudes smaller than 40 kPa confirming the results found by another set of authors.[10,29,32–35]

Figure 6 shows a typical example of an ultra high-speed recording of a microbubble with an initial bubble radius of 3.8 μm. The bubble was excited with 12 different frequencies near two times its resonance frequency, which was 1.3 MHz following van der Meer *et al.*[28] The subharmonic response is clearly visible both in the time and frequency domain.

We observe a maximum for the relative amplitude of the subharmonic response around a driving pressure frequency of 2.4 MHz corresponding to a 1.2 MHz subharmonic oscillation. At this frequency the amplitude of the (radial) subharmonic response is even higher than the amplitude of the fundamental response. One should keep in mind that here we display the radial response of the bubble. The acoustic response of the bubble, including its subharmonic component, can be directly calculated from the radial response, see e.g. Ref. 48. Based on conservation of mass and momentum one

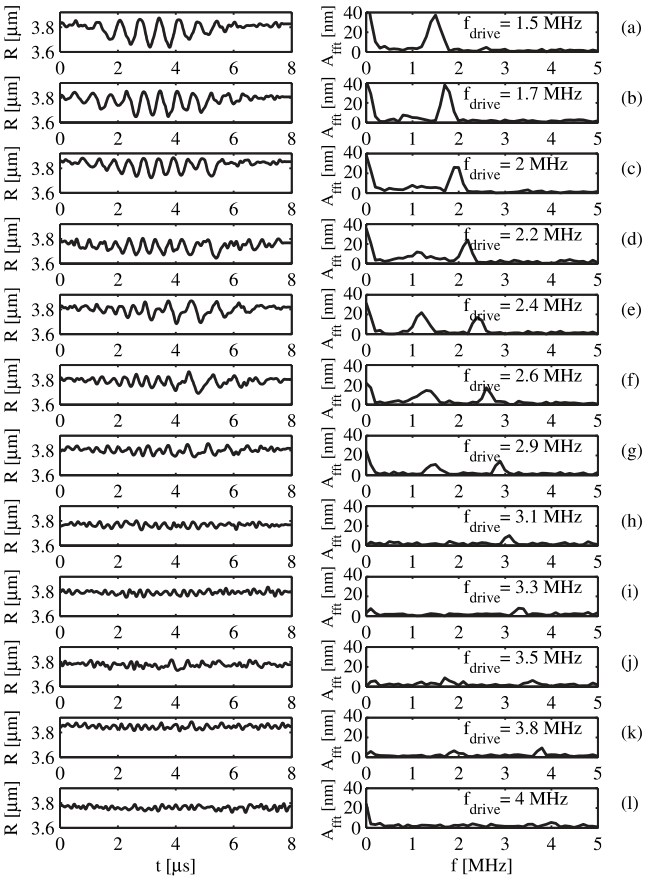

FIG. 6. The radius-time curves (left column) of a 3.8 μm microbubble excited with twelve different driving pulses all with an amplitude of 40 kPa and different frequencies. In the corresponding absolute value of the Fourier transform (sampling rate 50 MHz, length pulse 501 points) of the radius-time curves (right column) we observe clear subharmonic behavior. We can identify a subharmonic resonance curve that peaks at a driving frequency of 2.4 MHz, about twice the resonance frequency of the bubble.

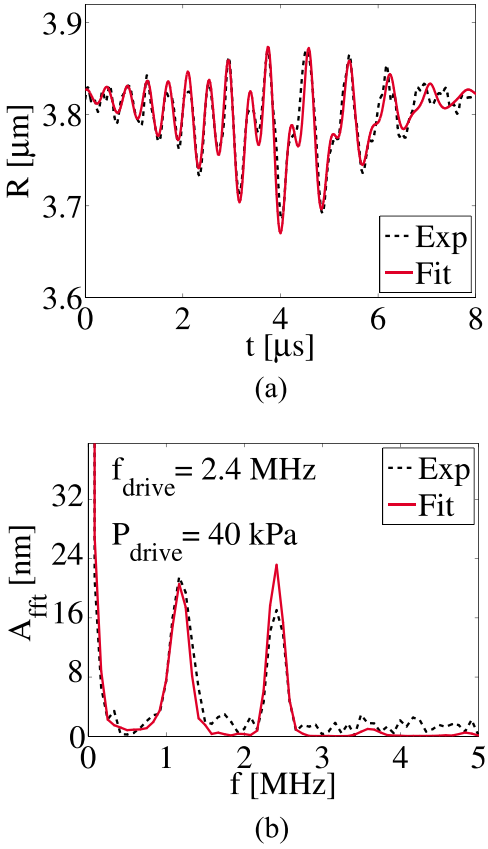

FIG. 7. (Color online) The best fit of the fifth radius-time curve from Fig. 6(e) with the model proposed by Marmottant *et al.* with the shell parameters $\chi_{max}=2.5$ N/m, $\zeta=2000$ N/m $\kappa_s=3\times10^{-8}$ (kg/s) and $\sigma(R_0)=0.001$ N/m both in (a) the time domain and (b) in the frequency domain (sampling rate both curves 50 MHz, 501 points).

can deduce that the subharmonic pressure amplitude will be decreased by a factor of four as compared to the fundamental echo amplitude.

Both above and below the resonance frequency the subharmonic response decreases and a subharmonic resonance curve (data not shown) can be obtained similar to the resonance curve produced with microbubble spectroscopy by van der Meer *et al.*[28] Furthermore, as expected, the fundamental response of the microbubble does not show a resonance behavior since it is excited far above its resonance frequency, which also explains why the fundamental response is observed to decrease for increasing driving pulse frequency. Finally, note that most of the responses presented in Fig. 6 show a zero order frequency component even though the initial bubble radius was subtracted from the radius-time curve before the Fourier transform was performed. The zero order component results from the compression-only behavior of the bubble, i.e., the bubble appears to compress more than it expands.[49,50]

The experimental data is compared to the theoretical predictions. Figure 7 shows a best fit of the model of Marmottant *et al.*[38] for the radius-time curve that shows the maximum subharmonic response in Fig. 6(e). The unknown parameters of the model, ζ, the shell viscosity κ_s and the initial surface tension $\sigma(R_0)$ of the bubble are varied using the iterative fit function *fit* in Matlab. The driving pressures for the simulated and measured radius-time curve are identical. The goal of the fit was not to determine the definitive values for the three shell parameters but to see if the model proposed by Marmottant *et al.* is able to predict subharmonic behavior of coated microbubbles at these low driving pressure amplitudes as observed in the experiments.

The agreement between the two radius-time curves is very good. It can be appreciated that the oscillation amplitude at the subharmonic frequency is of the same order as that at the fundamental frequency with a value of 5% of the initial bubble radius at the driving pressure amplitude of 40 kPa. The best fit parameters found are in good agreement with the parametric study presented in Sec. II B and the values found elsewhere in the literature. The best fit value for the shell viscosity $\kappa_s=3\times10^{-8}$ kg/s is in agreement with van der Meer *et al.*[28] To explain the amplitude of the subharmonic oscillations observed in Fig. 7 we observe in Fig. 4 that the amount of damping depicted by $\kappa_s=3\times10^{-8}$ kg/s requires a large value for ζ. Based on the experimentally measured relation between surface tension and phospholipid surface concentrations found in the literature the magnitude of ζ is expected to be at least three orders of magnitude larger than χ in order to explain the abrupt elasticity change

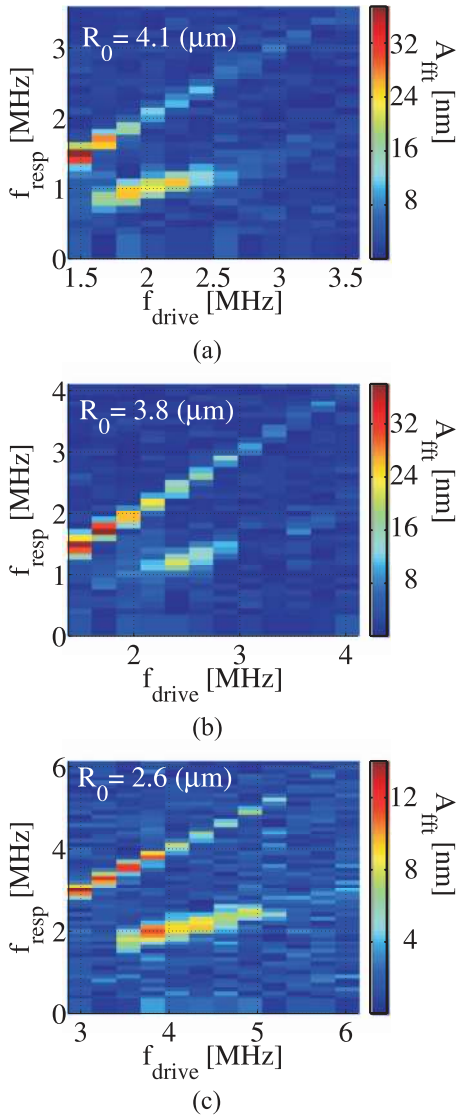

FIG. 8. The amplitude of the Fourier transform of the radial response of three differently sized bubbles as measured with the Brandaris ultra high-speed camera represented by a color. The horizontal axis represents twelve different driving pressure frequencies with a fixed driving pressure amplitude of 40 kPa. The response frequency is represented by the vertical axis.

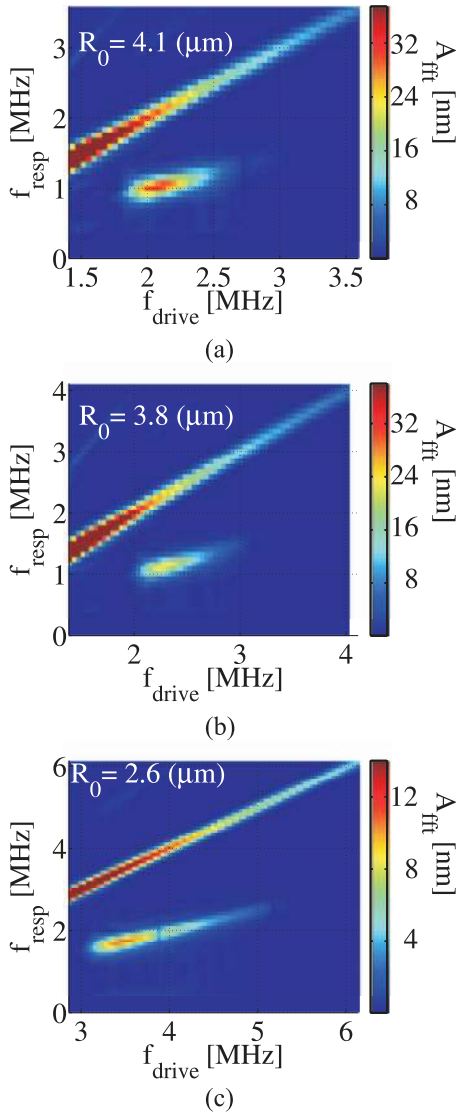

FIG. 9. Simulated subharmonic resonance behavior of coated microbubbles with the same initial bubble radii as in Fig. 8 using the best fit shell parameters found in Fig. 7

found for collapsing phospholipid monolayers.[43,44] This is in agreement with the value for ζ found in the best fit, namely $\zeta=2000$ N/m. Furthermore, in Sec. II B and from the analytical solutions in Sec. II A, we found $\sigma(R_0)$ should be close to zero which agrees well with the best fit value found in Fig. 7, $\sigma(R_0)=0.001$ N/m.

To investigate the frequency dependence of the subharmonic behavior of phospholipid coated microbubbles we varied the driving frequency as shown in Fig. 6. An overview of the frequency behavior presented in Fig. 6 is shown as a single plot in the spectrogram in Fig. 8(b). The horizontal axis of the figure is divided into twelve columns representing the twelve driving frequencies. The vertical axis represents the response frequencies corresponding to the horizontal axis of the figures in the right column of Fig. 6. A frequency of 50 MHz was used to interpolate the radius-time curves. The color coding in Fig. 8 represents the absolute value of the Fourier transform of the radius-time curves. The zero order frequency component was filtered out completely. Two other spectrograms for different bubble radii are presented in Figs. 8(a) and 8(c).

Figure 9 shows the full (sub)harmonic resonance behavior of the very same bubbles presented in Fig. 8. The initial surface tension and ζ were assumed to be equal to the values found in the previous fit (see Fig. 7) and the shell viscosity was assumed to vary with initial bubble radius as shown by van der Meer *et al.*[28] The color coding for the simulated spectra is identical to those in Fig. 8 allowing for a quantitative comparison between the experimental an theoretical subharmonic behavior. Both the simulated spectra and the measured spectra show subharmonic resonance behavior at the same frequencies. Furthermore, we identify a good agreement between the absolute amplitude of the subharmonic response between the simulated and the measured spectra.

To determine the threshold pressure for the initiation of subharmonic oscillations for coated bubbles the experiment as presented in Fig. 6 was repeated for different driving pressure amplitudes. The maximum response frequency for the

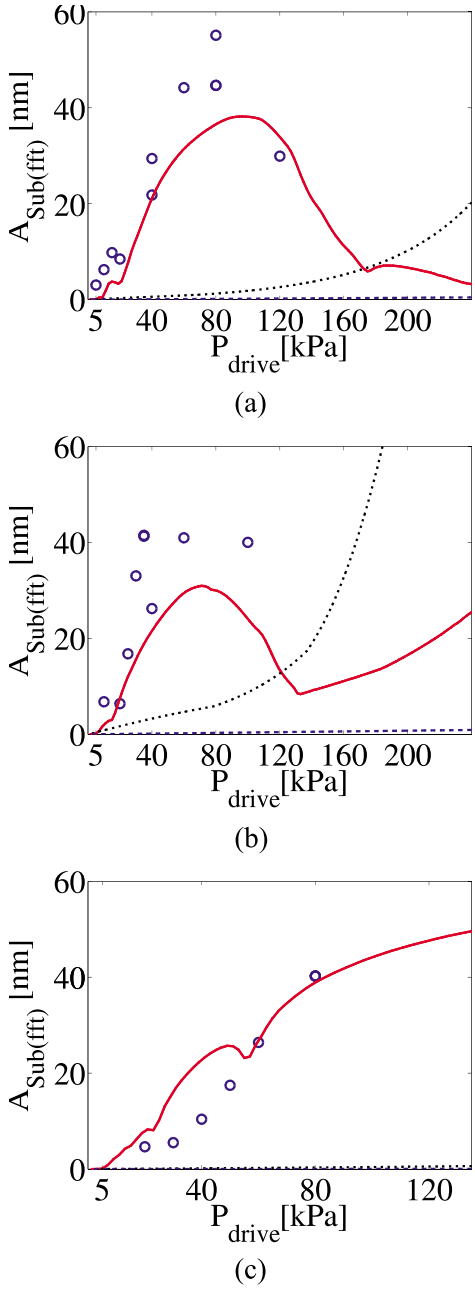

FIG. 10. (Color online) The maximum amplitude of the subharmonic oscillations of a (a) 3.8 μm, (b) 4.8 μm and (c) 2.4 μm bubble as a response to different driving pressure amplitudes. The measured responses are compared with the subharmonic responses for the same initial bubble radii predicted by three different models. The model proposed by Marmottant *et al.*[38] (solid line), and a purely linear viscoelastic shell model (dashed line) and a free gas bubble model (dotted line).

experimentally determined subharmonic oscillations was observed to decrease from 1.4 MHz (<5 kPa) to 1 MHz (>80 kPa) for increased driving pressures. This can be attributed to a non-linear phenomenon, where the frequency of maximum response of the bubble decreases for increased driving pressure.[18,42] In Fig. 10(a), the subharmonic oscillation amplitude at the maximum subharmonic response frequency is plotted as a function of the driving pressure amplitude. We observe that the threshold pressure for the initiation of subharmonic oscillations is smaller than 5 kPa, much lower than that of a free gas bubble without a shell and much lower than is expected based on the additional damping introduced by the phospholipid shell of the bubble.[10,29,32–35] For the 5 kPa driving pressure the only driving frequency showing a subharmonic response was 2.8 MHz corresponding to a resonance frequency of 1.4 MHz.

Interestingly, we observe that the subharmonic amplitude decreases for increasing driving pressure amplitudes above a pressure of 80 kPa. To investigate these results in more detail we conducted numerical simulations using three different models, a free gas bubble model as described by Lotsberg *et al.*,[32] a purely linear viscoelastic shell model[26] and the model proposed by Marmottant *et al.*[38] The shell parameters for the model of Marmottant *et al.* were taken from the best fit from Fig. 7. For the linear viscoelastic shell model we used the very same shell viscosity. The shell elasticity was taken from van der Meer *et al.*,[28] χ_{eff}=0.55 N/m, who determined the shell elasticity for a linear viscoelastic shell model. The initial surface tension in the linear viscoelastic shell model is assumed to be the same as found in the best fit from Fig. 7. In the numerical simulations, the initial bubble radius and driving pressures were those of the experiments. As discussed before, the maximum subharmonic/linear response frequency varies slightly for increased driving amplitudes. Therefore, similar to the experiments, we varied the driving frequency around twice the resonance frequency of the bubble to find the maximum subharmonic response frequency. The maximum subharmonic oscillation amplitude for the three different models at the maximum subharmonic response frequency was plotted against the driving pressure amplitude together with the experimental data in Fig. 10(a). From this figure it is clear that the free gas bubble model starts to show subharmonic behavior for driving pressure amplitudes between 50 and 80 kPa whereas the experimental data shows subharmonic behavior already at a driving pressure amplitudes of 5 kPa. As a result of the increased damping introduced by the bubble shell, the linear viscoelastic shell model shows no subharmonics up to a driving pressure amplitude of 240 kPa. The model by Marmottant *et al.* on the other hand predicts that the threshold pressure for the initiation of subharmonics almost vanishes, which is in agreement with what is found experimentally. Overall the agreement between the theoretical predictions of the model proposed by Marmottant *et al.*[38] and the experimental data is very good. Also the decrease of the subharmonic oscillation amplitude for higher pressures seems to be correctly predicted by the model. The very same experiments and numerical simulations were conducted for two other microbubbles: one for a bubble with an initial bubble radius of 4.8 μm and one for a 2.4 μm radius bubble; these are presented in Figs. 10(b) and 10(c), respectively. The shell viscosity was adapted to the initial bubble radius of the bubble in accordance with the results of van der Meer *et al.*,[28] who found a shell viscosity depending on bubble size, or more precisely on dilatation rate. The shell viscosity was directly taken from Fig. 8(b) from van der Meer *et al.*[28] For the 4.8 μm radius bubble the shell viscosity was therefore taken to be equal to 4.3×10^{-8} kg/s and for the 2.4 μm radius bubble it was taken to be equal to 1.2×10^{-8} kg/s.

In Figs. 10(c) and 10(b), we again observe that the subharmonic threshold pressure has decreased considerably compared to the threshold pressure predicted for a free gas bubble of the same size. The linear viscoelastic shell model is unable to predict subharmonics at such low driving pressure amplitudes.

Figures 10(a)–10(c) show that the subharmonic oscillation amplitude of the largest and smallest bubble is of comparable magnitude. Furthermore it is found that the threshold pressure for the initiation of subharmonic oscillations does not vary strongly with bubble radius. We also observe that for all three bubble sizes the model of Marmottant *et al.* predicts a maximum for the subharmonic oscillation amplitude between a driving pressure of 50 and 100 kPa.

V. DISCUSSION

From the comparison between the analytical, numerical and experimental results we conclude that the subharmonic behavior of phospholipid coated microbubbles at low acoustic driving pressure amplitudes can be explained by a rapid change of the effective surface tension of the bubble shell. We also find that the subharmonic behavior of phospholipid coated microbubbles is predominantly determined by the initial phospholipid surface concentration on the bubble wall. The description of the effective surface tension of a phospholipid coated microbubble as a function of bubble radius proposed by Marmottant *et al.*[38] is based on the quasi-static behavior of phospholipid monolayers.[51,52] Here we show that the main features of the model responsible for the subharmonic behavior of phospholipid coated microbubbles, such as the large change of the initial shell elasticity, also provide excellent agreement with experimental observations at higher frequencies. The phospholipid molecules covering the surface of BR-14 microbubbles, are distearoylphosphatidylcholine (DSPC), and dipalmytoylphosphatidylglycerol (DPPG). These are well known pulmonary surfactants[53] and their dynamic behavior has been the subject of numerous studies. Hereto, researchers make use of a so-called pulsating bubble surfactometer.[54] In a pulsating bubble surfactometer a bubble of around 500 μm is coated with the surfactant of interest while the radius of the bubble is varied through an externally applied pressure. The pressure in and outside the bubble, which is monitored during the oscillations, provides direct information on the dynamic surface tension of the bubble. From dynamic surface tension measurements conducted by Wen *et al.*[43] and Cheng *et al.*[44] on DPPC (similar to DPPG and DSPC) we observe that the change of the shell elasticity is indeed much larger than the shell elasticity itself for an initial surface tension close to the phospholipid surface saturation concentration (which can be appreciated from the sharp peaks for low effective surface tension and round peaks for large effective surface tension in Fig. 2 of Ref. 43 and Fig. 1 of Ref. 44.

The functional form of the effective surface tension figure proposed by Marmottant *et al.*[38] is based on a few approximations: a perfectly elastic regime can be defined, the elasticity is zero in the buckled regime and after rupture of the shell, buckling and rupture are reversible, the surface tension goes to zero in the buckled state. Furthermore, a more realistic description should account for several factors that are known to influence the dynamic behavior of phospholipids monolayer, such as the ionic strength and pH of the solution, temperature, impurities and dissolved surfactants.[53]

An explanation why around 50% of the microbubbles studied in this paper and similar studies by other authors[36,37] showed no subharmonic behavior at low acoustic driving pressures could be that the surface of these bubbles was insufficiently saturated with phospholipids. This would result in an insufficiently large change of the initial shell elasticity to initiate subharmonic behavior.

The findings presented in this paper are valuable for the application of phospholipid coated microbubbles in medical ultrasound imaging. By controlling the initial conditions of the microbubbles, their subharmonic behavior can be enhanced leading to an improved contrast to tissue ratio in contrast-enhanced ultrasound imaging. One way of changing and controlling the initial conditions of the phospholipid shell is through a change of the ambient pressure. This idea has very recently been shown by Frinking *et al.*[55] and provides new possibilities for non-invasive *in vivo* hydrostatic pressure estimations inside the heart and large vessels.

VI. CONCLUSIONS

Through a weakly non-linear analysis we provided an explanation for the decrease of the threshold amplitude of the driving pressure above which the subharmonic behavior of phospholipid coated microbubbles is initiated. We show that a decrease of the subharmonic threshold for coated microbubbles can only be explained if the shell elasticity of the bubble shell, $\chi(R)$, varies rapidly with the amplitude of oscillation. Unlike the purely linear viscoelastic models[26,27,30,31] the model of Marmottant *et al.*[38] assumes that the shell of a phospholipid coated microbubble is elastic only in a small radius domain. Outside this domain the shell elasticity is zero. It is shown that as a result of this rapid change in the shell elasticity, the subharmonic behavior of coated microbubbles is likely to occur already for driving pressure amplitudes as low as 6 kPa.

In a full parametric study of the model we show that the initial surface tension of the bubble shell, i.e., the initial phospholipid surface concentration, determines whether or not subharmonics occur. If the initial surface tension of the bubble is sufficiently close to the buckled regime and the collapse of the phospholipid monolayer from the elastic regime to the buckled regime determined by ζ is sufficiently abrupt subharmonic behavior is enhanced. Furthermore it is confirmed that the subharmonic behavior is enhanced for a smaller shell viscosity.

Experimentally the subharmonic radial dynamics of differently sized microbubbles was studied for different driving pressure frequencies near two times the resonance frequency of the bubble for different driving pressure amplitudes. Subharmonic oscillations were observed for bubbles insonified with driving pressures with amplitudes as low as 5 kPa. This indicates that the threshold pressure above which subharmonic oscillations may occur is even smaller for phospho-

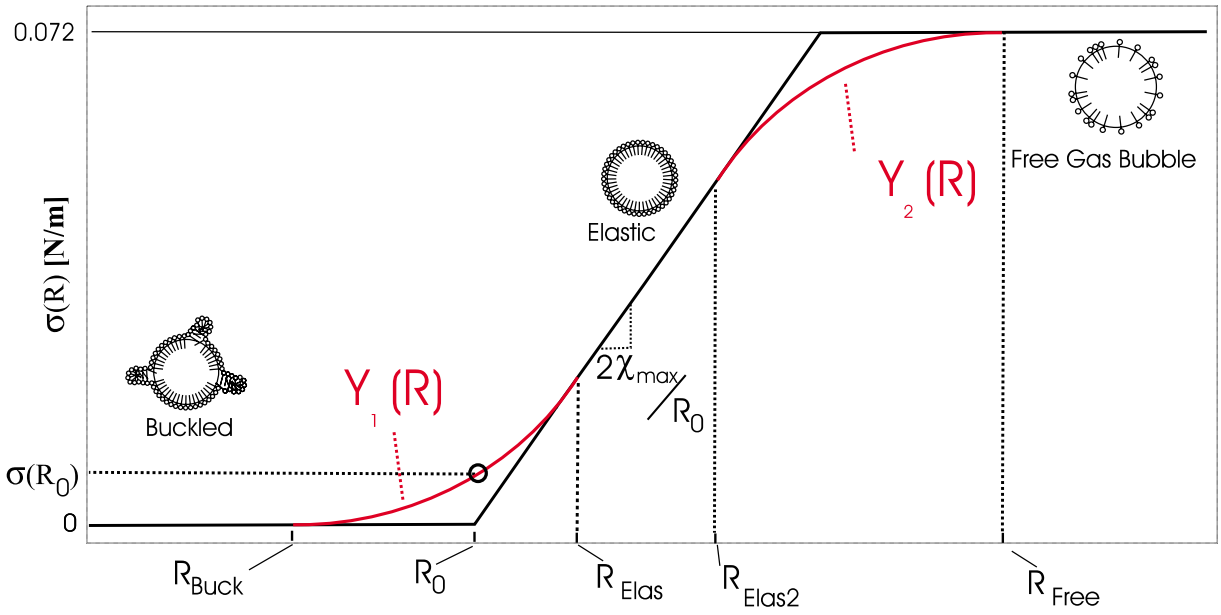

FIG. 11. (Color online) In the model of Marmottant *et al.*[38] the second derivative of $\sigma(R)$ with respect to R is undefined in the transitions from the buckled regime to the elastic regime, and from the elastic regime to the free gas bubble regime. To correct this, we propose to expand the original model with two quadratic functions Y_1 and Y_2 that describe the two transition points.

lipid coated microbubbles than for free gas bubbles, even though as a result of the shell viscosity coated bubbles are more heavily damped.

ACKNOWLEDGMENTS

We thank A. Prosperetti and H.J. Vos for stimulating discussions. G.W. Bruggert and M. Bos are acknowledged for the technical support. Bracco Research SA is acknowledged for the supply of the BR-14 ultrasound contrast agents.

APPENDIX

As a first approximation Marmottant *et al.*[38] assumed three regimes for $\sigma(R)$, an elastic regime, for small bubble oscillations and two regimes where the shell elasticity is zero in accordance with the known quasi-static behavior of phospholipid monolayers. The shell elasticity χ in the elastic regime is assumed to be constant and the function $\sigma(R)$ as a whole is assumed to be identical for all bubbles independent of the initial bubble radius. Therefore this model introduces only one additional parameter as compared to the model proposed by de Jong *et al.*:[26] the initial surface tension of the bubble $\sigma(R_0)$, which directly relates to the phospholipid concentration on the interface of the bubble.

In the model described by Marmottant *et al.* $\sigma(R)$ is defined as a piecewise affine function, implying that $\zeta(R)$, i.e., the derivative of $\chi(R)$ with respect to R is zero except at the two transition points $\sigma(R)=0$ and $\sigma(R)=\sigma_{\text{water}}$, where this quantity is not defined. As already pointed out by Marmottant *et al.*,[38] this is a practical idealization of the shell response which is smoother in reality.

In the original model ζ was undefined in the two transition regions. With the introduction of the two quadratic function the constant ζ can now be defined. This suggests that a new shell parameter must be introduced, however, since in the original model ζ was undefined, and was in fact determined by the step size of the numerical solution of the Rayleigh-Plesset equation, the original model could also be considered as having already incorporated (in an uncontrolled way) the ζ shell parameter.

In order to have $\zeta(R)$ defined for all R we propose to introduce two quadratic crossover functions, $Y_1(R)$ and $Y_2(R)$ in the two transition regions as depicted in Fig. 11. In order for both the effective surface tension and the shell elasticity to remain continuous at the two transition points the two quadratic functions at the two different transitions should each satisfy a set of boundary conditions. For the transition from the so called buckled regime to the elastic regime the function $Y_1(R)$ should be chosen such that $\sigma(R)$ satisfies

$$\sigma(R_{\text{Buck}}) = 0 \ \text{N/m},$$

$$\partial\sigma(R_{\text{Buck}})/\partial R = 0 \ \text{N/m}^2,$$

$$\partial\sigma(R_{\text{Elas}})/\partial R = 2\chi_{\max}/R_0 \ \text{N/m}^2, \tag{A1}$$

where R_{Buck} marks the transition to the buckled regime and R_{Elas} to the elastic regime. In a separate experiment by Overvelde *et al.*[42] resonance curves of phospholipid coated BR-14 microbubbles were measured at very low driving pressures. This allowed for measurements of the resonance curves of a bubble in a purely elastic state as the oscillations were confined to the elastic regime. In this way the *maximum* shell elasticity in the elastic regime could be determined and was found to be $\chi_{\max}=2.5$ N/m. For radii between R_{Buck} and R_{Elas} the shell elasticity is determined by Y_1 as shown in Fig. 11. To limit the number of free parameters of the model we have assumed the transition from the buckled regime to the elastic regime and from the elastic regime to the ruptured regime to be identical. The boundary conditions that should

be satisfied for this latter transition are therefore

$$\sigma(R_{\text{Free}}) = 0.072 \ \text{N/m},$$

$$\partial\sigma(R_{\text{Elas2}})/\partial R = 2\chi_{\max}/R_0 \ \text{N/m}^2,$$

$$\partial\sigma(R_{\text{Free}})/\partial R = 0 \ \text{N/m}^2. \tag{A2}$$

The end of the elastic regime is now marked by R_{Elas2} and the start of the ruptured regime is marked by R_{free}. From the boundary conditions we find the following quadratic functions:

$$Y_1 = \frac{1}{2}\zeta\left(\frac{R}{R_{\text{Buck}}} - 1\right)^2 \quad \text{for} \quad R_{\text{Buck}} < R < R_{\text{Elas}}, \tag{A3}$$

$$Y_2 = \sigma_{\text{water}} - \frac{1}{2}\zeta\left(\frac{R}{R_{\text{Buck}}} - \frac{R_{\text{Free}}}{R_{\text{Buck}}}\right)^2 \quad \text{for} \quad R_{\text{Elas2}} < R < R_{\text{Free}}. \tag{A4}$$

With these two new quadratic functions the final function of $\sigma(R)$ becomes

$$\sigma(R) = \begin{cases} 0 & R < R_{\text{Buck}} \\ Y_1(R) & R_{\text{Buck}} < R < R_{\text{Elas}} \\ 2\chi_{\max}\left(\frac{R}{R_0} - 1\right) & R_{\text{Elas}} < R < R_{\text{Elas2}} \\ Y_2(R) & R_{\text{Elas2}} < R < R_{\text{Free}} \\ \sigma_{\text{water}} & R > R_{\text{Free}}. \end{cases} \tag{A5}$$

Note that in this model the initial effective surface tension of $\sigma(R_0)$ is adjusted by shifting the function of $\sigma(R)$ horizontally while fixing R_0, see Fig. 11.

[1]F. Forsberg, D. A. Merton, J. B. Liu, L. Needleman, and B. B. Goldberg, "Clinical applications of ultrasound contrast agents," Ultrasonics **36**, 695–701 (1998).
[2]T. Albrecht and J. Hohmann, "Ultrasound contrast agents," Radiologe **43**, 793–804 (2003).
[3]F. B. Feinstein, "The powerful microbubble: From bench to bedside, from intravascular indicator to therapeutic delivery system, and beyond," Am. J. Physiol. Heart Circ. Physiol. **287**, H450–457 (2004).
[4]B. A. Kaufmann and J. R. Lindner, "Molecular imaging with targeted contrast ultra sound," Curr. Opin. Biotechnol. **18**, 11–16 (2007).
[5]A. Bouakaz, S. Frigstad, F. J. ten Cate, and N. de Jong, "Super harmonic imaging: A new imaging technique for improved contrast detection," Ultrasound Med. Biol. **28**, 59–68 (2002).
[6]V. Mor-Avi, E. G. Caiani, K. A. Collins, C. E. Korcarz, J. E. Bednarz, and R. M. Lang, "Combined assessment of myocardial perfusion and regional left ventricular function by analysis of contrast-enhanced power modulation images," Circulation **104**, 352–357 (2001).
[7]D. H. Simpson, C. T. Chin, and P. N. Burns, "Pulse inversion Doppler: A new method for detecting nonlinear echoes from microbubble contrast agents," IEEE Trans. Ultrason. Ferroelectr. Freq. Control **46**, 372–382 (1999).
[8]P. J. A. Frinking, A. Bouakaz, J. Kirkhorn, F. J. ten Cate, and N. de Jong, "Ultrasound contrast imaging: Current and new potential methods," Ultrasound Med. Biol. **26**, 965–975 (2000).
[9]P. Rafter, P. Phillips, and M. A. Vannan, "Imaging technologies and techniques," Cardiol. Clin. **22**, 181–197 (2004).
[10]P. M. Shankar, P. D. Krishna, and V. L. Newhouse, "Advantages of subharmonic over second harmonic backscatter for contrast-to-tissue echo enhancement," Ultrasound Med. Biol. **24**, 395–399 (1998).
[11]D. E. Goertz, M. E. Frijlink, N. de Jong, and A. F. W. van der Steen, "High frequency nonlinear scattering from a micrometer to submicrometer sized lipid encapsulated contrast agent," Ultrasound Med. Biol. **32**, 569–577 (2006).
[12]D. E. Goertz, M. E. Frijlink, D. Tempel, V. Bhagwandas, A. Gisolf, R. Krams, N. de Jong, and A. F. W. van der Steen, "Subharmonic contrast intravascular ultrasound for vasa vasorum imaging," Ultrasound Med. Biol. **33**, 1859–1872 (2007).
[13]R. Esche, "Investigations on oscillating cavities in liquids," Acustica **2**, 208–218 (1952).
[14]E. A. Neppiras, "Subharmonic and other low-frequency emission from bubbles in sound-irradiated liquids," J. Acoust. Soc. Am. **46**, 587–601 (1969).
[15]P. de Santis, D. Sette, and F. Wanderlingh, "Cavitation detection: The use of the subharmonics," J. Acoust. Soc. Am. **42**, 514–516 (1967).
[16]A. Eller and H. G. Flynn, "Generation of subharmonics of order one-half by bubbles in a sound field," J. Acoust. Soc. Am. **46**, 722–727 (1969).
[17]A. I. Eller, "Subharmonic response of bubbles to underwater sound," J. Acoust. Soc. Am. **55**, 871–873 (1974).
[18]A. Prosperetti, "Nonlinear oscillations of gas bubbles in liquids: Steady-state solutions," J. Acoust. Soc. Am. **56**, 878–885 (1974).
[19]A. Prosperetti, "Nonlinear oscillations of gas bubbles in liquids. Transient solutions and the connection between subharmonic signal and cavitation," J. Acoust. Soc. Am. **57**, 810–821 (1975).
[20]W. Lauterborn, "Numerical investigation of nonlinear oscillations of gas bubbles in liquids," J. Acoust. Soc. Am. **59**, 283–293 (1976).
[21]M. S. Plesset and A. Prosperetti, "Bubble dynamics and cavitation," Annu. Rev. Fluid Mech. **9**, 145–185 (1977).
[22]T. G. Leighton, *The Acoustic Bubble* (Academic, London, 1994).
[23]C. E. Brennen, *Cavitation and Bubble Dynamics* (Oxford University Press, Oxford, 1995).
[24]M. Brenner, S. Hilgenfeldt, and D. Lohse, "Single-bubble sonoluminescence," Rev. Mod. Phys. **74**, 425–484 (2002).
[25]A. Prosperetti, "Application of the subharmonic threshold to the measurement of the damping of oscillating gas bubbles," J. Acoust. Soc. Am. **61**, 11–16 (1977).
[26]N. de Jong and L. Hoff, "Ultrasound scattering properties of Albunex microspheres," Ultrasonics **31**, 175–181 (1993).
[27]K. Sarkar, W. T. Shi, D. Chatterjee, and F. Forsberg, "Characterization of ultrasound contrast microbubbles using in vitro experiments and viscous and viscoelastic interface models for encapsulation," J. Acoust. Soc. Am. **118**, 539–550 (2005).
[28]S. van der Meer, B. Dollet, M. Voormolen, C. T. Chin, A. Bouakaz, N. de Jong, M. Versluis, and D. Lohse, "Microbubble spectroscopy of ultrasound contrast agents," J. Acoust. Soc. Am. **121**, 648–656 (2007).
[29]P. M. Shankar, P. D. Krishna, and V. L. Newhouse, "Subharmonic backscattering from ultrasound contrast agents," J. Acoust. Soc. Am. **106**, 2104–2110 (1999).
[30]C. C. Church, "The effect of an elastic solid surface layer on the radial pulsations of gas bubbles," J. Acoust. Soc. Am. **97**, 1510–1521 (1995).
[31]L. Hoff, P. C. Sontum, and J. M. Hovem, "Oscillations of polymeric microbubbles: Effect of the encapsulating shell," J. Acoust. Soc. Am. **107**, 2272–2280 (2000).
[32]O. Lotsberg, J. M. Hovem, and B. Aksum, "Experimental observation of subharmonic oscillations in Infoson bubbles," J. Acoust. Soc. Am. **99**, 1366–1369 (1996).
[33]P. D. Krishna, P. M. Shankar, and V. L. Newhouse, "Subharmonic generation from ultrasonic contrast agents," Phys. Med. Biol. **44**, 681–694 (1999).
[34]P. H. Chang, K. K. Shung, S. Wu, and H. B. Levene, "Second harmonic imaging and harmonic Doppler measurements with Albunex," IEEE Trans. Ultrason. Ferroelectr. Freq. Control **42**, 1020–1027 (1995).
[35]E. Biagi, L. Breschi, E. Vannacci, and L. A. Masotti, "Stable and transient subharmonic emissions from isolated contrast agent microbubbles," IEEE Trans. Ultrason. Ferroelectr. Freq. Control **54**, 480–497 (2007).
[36]G. Bhagavatheeshwaran, W. T. Shi, F. Forsberg, and P. M. Shankar, "Subharmonic signal generation from contrast agents in simulated neovessels," Ultrasound Med. Biol. **30**, 199–203 (2004).
[37]E. Kimmel, B. Krasovitski, A. Hoogi, D. Razansky, and D. Adam, "Subharmonic response of encapsulated microbubbles: Conditions for existence and amplification," Ultrasound Med. Biol. **33**, 1767–1776 (2007).
[38]P. Marmottant, S. van der Meer, M. Emmer, M. Versluis, N. de Jong, S. Hilgenfeldt, and D. Lohse, "A model for large amplitude oscillations of coated bubbles accounting for buckling and rupture," J. Acoust. Soc. Am. **118**, 3499–3505 (2005).
[39]C. T. Chin, C. Lancée, J. Borsboom, F. Mastik, M. E. Frijlink, N. de Jong, M. Versluis, and D. Lohse, "Brandaris 128: A digital 25 million frames per second camera with 128 highly sensitive frames," Rev. Sci. Instrum. **74**,

5026–5034 (2003).
[40]C. Devin, Jr., "Survey of thermal, radiation and viscous damping of pulsating bubbles," J. Acoust. Soc. Am. **31**, 1654–1667 (1959).
[41]H. Medwin, "Counting bubbles acoustically: A review," Ultrasonics **15**, 7–13 (1977).
[42]M. Overvelde, V. Garbin, J. Sijl, B. Dollet, N. de Jong,, D. Lohse, and M. Versluis, "Nonlinear shell behavior of phospholipid-coated microbubbles," Ultrasound Med. Biol. (2010, in print).
[43]X. Wen and E. I. Franses, "Adsorption of bovine serum albumin at the air/water interface and its effect on the formation of DPPC surface film," Colloids Surf., A **190**, 319–332 (2001).
[44]C. C. Cheng and C.-H. Chang, "Retardation effect of tyloxapol on inactivation of dipalmitoyl phosphatidylcholine surface activity by albumin," Langmuir **16**, 437–441 (2000).
[45]J. Sijl, E. Gaud, P. J. A. Frinking, M. Arditi, N. de Jong, D. Lohse, and M. Versluis, "Acoustic characterization of single ultrasound contrast agent microbubbles," J. Acoust. Soc. Am. **124**, 4091–4097 (2008).
[46]V. Garbin, D. Cojoc, E. Ferrari, E. Di Fabrizio, M. L. J. Overvelde, S. M. van der Meer, N. de Jong, D. Lohse, and M. Versluis, "Changes in microbubble dynamics near a boundary revealed by combined optical micromanipulation and high-speed imaging," Appl. Phys. Lett. **90**, 114103 (2007).
[47]B. Dollet, S. van der Meer, V. Garbin, N. de Jong, D. Lohse, and M. Versluis, "Nonspherical oscillations of ultrasound contrast agent microbubbles," Ultrasound Med. Biol. **34**, 1465–1473 (2008).
[48]S. Hilgenfeldt, D. Lohse, and M. Zomack, "Response of bubbles to diagnostic ultrasound: A unifying theoretical approach," Eur. Phys. J. B **4**, 247–255 (1998).
[49]N. de Jong, M. Emmer, C. T. Chin, A. Bouakaz, F. Mastik, D. Lohse, and M. Versluis, "'Compression-only' behavior of phospholipid-coated contrast bubbles," Ultrasound Med. Biol. **33**, 653–656 (2007).
[50]J. Sijl, M. Overvelde, B. Dollet, V. Garbin, N. de Jong, D. Lohse, and M. Versluis, "'Compression-only' behavior: A second order nonlinear response of ultrasound contrast agent microbubbles," J. Acoust. Soc. Am. (2010, in print).
[51]M. I. Sández, A. Suárez, and A. Gil, "Surface pressure-area isotherms and fluorescent behavior of phospholipids containing labeled pyrene," J. Colloid Interface Sci. **250**, 128–133 (2002).
[52]F. Pétriat, E. Roux, J. C. Leroux, and S. Giasson, "Study of molecular interactions between a phospholipidic layer and a pH-sensitive polymer using the Langmuir balance technique," Langmuir **20**, 1393–1400 (2004).
[53]R. Veldhuizen, K. Nag, S. Orgeig, and F. Possmayer, "The role of lipids in pulmonary surfactant," Biochim. Biophys. Acta **1408**, 90–108 (1998).
[54]G. Enhorning, "Pulsating bubble technique for evaluating pulmonary surfactant," J. Appl. Physiol. **43**, 198–203 (1977).
[55]P. J. A. Frinking, E. Gaud, J. Brochot, and M. Arditi, "Subharmonic scattering of phospholipid-shell microbubbles at low acoustic pressure amplitudes," IEEE Trans. Ultrason. Ferroelectr. Freq. Control **57**, 1762–1771 (2010).